Hindawi
International Journal of Chemical Engineering
Volume 2023, Article ID 8892450, 13 pages
https://doi.org/10.1155/2023/8892450

Research Article

Performance Improvement of OTEC-ORC and Turbine Based on Binary Zeotropic Working Fluid

Qingfen Ma,[1] **Jie Huang**,[1] **Zezhou Gao**,[1] **Hui Lu**,[2] **Hongfeng Luo**,[1] **Jingru Li**,[1] **Zhongye Wu**,[1] **and Xin Feng**[1]

[1]*College of Mechanical and Electrical Engineering, Hainan University, Haikou, Hainan 570228, China*
[2]*Institute of Environment and Plant Protection, Chinese Academy of Tropical Agriculture Sciences, Haikou, Hainan 571101, China*

Correspondence should be addressed to Hongfeng Luo; 990547@hainanu.edu.cn

Received 17 December 2022; Revised 20 January 2023; Accepted 9 February 2023; Published 8 March 2023

Academic Editor: Maciej Jaskulski

In this paper, the composition of binary nonazeotropic working fluids is explored from the perspective of improving OTEC-ORC efficiency, and the turbine is designed to accommodate with the working fluid. It is found that the OTEC-ORC using a R152a/R32 mixture as the working fluid is significantly higher than the OTEC-ORC thermal efficiency and system efficiency of the pure NH3, and the optimal composition of the mixed working fluid R152a/R32 is determined to be 85 : 15 with the thermal efficiency and the system efficiency of 2.8% and 1.7%, respectively, improving by 35.7% and 151.2% compared to the NH_3 ORC. According to the determined working fluid, a one-dimensional (1-D) design and CFD simulation analysis simulation are carried out on the turbine. The 1-D calculation results are in good agreement with the three-dimensional (3-D) results. At the design point, the turbine output is 83.84 kW, and the isentropic efficiency is 87.53%. At the off-design point, turbines have better off-design performance, indicating that the designed turbine also has good adaptability.

1. Introduction

The development and utilization of ocean thermal energy provide a way to solve the energy problem [1–5]. In existing studies, the thermal efficiency of the organic Rankine cycle (ORC) in the ocean thermal energy conversion (OTEC) system is very low, only 1.3%–3.5% [6–8]. The efficiency of the OTEC-ORC is inseparable from the working fluid. Ammonia is the most commonly used working fluid in OTEC-ORC due to its large enthalpy difference and easy accessibility [9]. Li et al. [10] used an ejector to improve system efficiency with ammonia fluid. Hasan and Dincer [6] used the ammonia Rankine cycle for regional cooling, ammonia, and electricity production. He et al. [11] studied the impact of ammonia, R22, R134a, R290, and R1270 on the OTEC power generation system. The results show that compared with R22, R134a, R290, and R1270, ammonia has the lowest circulating capacity, indicating it is suitable for the OTEC power generation system.

Vera et al. [12] investigated the influence of ammonia, R152a, R1234yf, R1234ze, R125, R134a, R161, propane, isobutene, RE143a, and decafluorobutane on net electric power. With respect to electric power, ammonia has the largest net output power and the lowest pumping losses, which makes it more suitable for OTEC-ORC. Zhang et al. [13] designed a 30 kW turbine with ammonia as the working fluid, and the isentropic efficiency of the turbine reached 85.2%. They also discovered the best ratio of blade tip clearance to inlet blade height is 0.04–0.06. Li et al. [14] studied the system performance of OTEC-ORC with R134a. The results show that the cycle thermal efficiency of the system is 5.15%. Yoon et al. [15] investigated the effects on system performance, utilizing ammonia, R404A, and R245fa, proving that ammonia had the greatest thermal efficiency in wet working fluids. Li and Zhang [16] used ammonia, R134a, and R600, respectively, to numerically analyze the effect of evaporation pressure on the performance of the system. The results indicated ammonia was

more suitable for OTEC-ORC, which had a higher thermal efficiency and a broader working range of evaporation pressure.

As a zeotropic mixture has a temperature glide during the phase transition process, which matches well with the temperature change of the heat source of OTEC to reduce the energy loss and improve the system efficiency and thermal efficiency [17]. Ammonia-water is the most commonly used zeotropic mixture. Kalina [18], Uehara [19], and Liu et al. [20] used ammonia-water to make the thermal efficiency reach 4.5%, 5%, and 5.16%, respectively. Liu et al. [21] summarized the influence of various zeotropic mixtures on the thermal efficiency and found that these could reduce the loss in the heat exchange process, so that the thermal efficiency of the system was improved. Yang and Yeh [22] investigated the performances of the OTEC system with R32/R717 and R1234YF/R717. The maximum net output powers of R717/R32 and R717/R2234YF were 18.9% and 12.23% higher than those of single ammonia at the mass fraction ratios of 0.21/0.79 and 0.41/0.59. When the mass fraction ratios were 0.4/0.6 and 0.62/0.38, the economic performances were 3.45% and 2.1% higher than that of pure R717, respectively. The above zeotropic mixture still has large wet degree due to the component of R717. Yang and Yeh [23] investigated the effects of R1123, R161, R32, and their mixtures on the performance of OTEC-ORC. The results show that the net power output and economy of the two-component mixture are better than those of the pure working fluid. The three-component mixture R1123/R161/R32 has the best performance among all the working fluids, and its net power output is about 52.36% higher than R1123, and its economic performance is about 32% higher than ammonia. From the perspective of environmental protection, our group [24] studied the performance of R1224yd(Z)/R1243zf as an OTEC-ORC working fluid. The results show that the optimal composition of R1224y/(Z)/R1243zf is 16 : 84, and the maximum thermal efficiency of the cycle reaches about 4.25%, proving R1224yd(Z)/R1243zf is an efficient working fluid that can replace pure NH_3 in the superheated state. Yoon et al. [25] discussed the OTEC system with R32/R152a. They had improved the efficiency of the system by 16% using liquid-steam ejectors. In addition, the systems with R32/R152a could reduce the size of evaporator and condenser by 13% and 14%, respectively, thereby reducing the initial cost. However, the low proportion of R152a will lead to the mixed working fluid deviating more from the isentropic working fluid. In addition, as the impact of climatic conditions deteriorates, environmental protection is also one of the important issues we need to consider. GWP is an index of the greenhouse effect produced by a substance, and the higher the index, the easier it is to cause the greenhouse effect. The GWP of R152a is about one-sixth that of R32, which is more environmentally friendly. Therefore, considering the above advantages of R152a, the composition of the mixture R152a/R32 should be further discussed for the goal of maximum system efficiency, considering the power consumption of the seawater pump, not just cycle thermal efficiency and turbine power.

Besides, with the change of working fluid in OTEC-ORC, the structure of the turbine also changes, so the matching design of the turbine should also be considered. As we have investigated, the research about ORC turbines mainly focuses on the design and simulation of turbines with pure working fluid, lacking the design and simulation of turbines mixed working fluids. Therefore, it is necessary to design and perform CFD simulation of a turbine with mixed working fluid to verify the output capacity and to provide methods for the design of such turbines.

Considering the comprehensive properties of working fluid, such as the thermodynamic parameters, safety, stability, and other characteristics, this paper preliminarily screens out the suitable components of working fluid for OTEC-ORC. The components and their proportions are determined by comparing the thermal efficiency and system efficiency with ammonia ORC. An OTEC turbine with 100 kW as the theoretical output power is designed through the simplified 1-D flow calculation and 3-D CFD simulation. The CFD simulations are carried out to investigate the influences of the operating conditions and reveal the off-design performance of the OTEC turbine using a R152a/R32 mixture as the working fluid.

2. Determination of Working Fluid

2.1. Design of the OTEC-ORC with Zeotropic Working Fluid. An OTEC-ORC with zeotropic working fluid is shown in Figure 1. It consists of an evaporator, a condenser, a working fluid pump, a turbine, cold and warm seawater pump. First, the working fluid pressurized by the working fluid pump is sent to the evaporator, where it is evaporated by the surface warm seawater to obtain a superheated saturated vapor after experiencing a temperature glide. Then the vapor promotes the turbine to rotate to generate power, and the exhausted steam from the turbine is expelled into the condenser to be condensed by the deep, cold seawater and finally sent to the working fluid pump to repeat the cycle.

Figure 2 shows a *T-S* diagram of the ORC with zeotropic working fluids. The steam-working fluid at point 1 can be saturated or overheated. Although the turbine in the saturated steam states is beneficial for the efficiency because a higher turbine inlet pressure can result in a larger pressure ratio [26], the turbine may be impacted and corroded by the droplets, increasing the operating risk and reducing the service life of the turbine [27]. Therefore, the superheated steam state is adopted in this study. Figure 2 also indicates that there should be a pinch point (usually set to 2°C [28]) between the temperature of warm and cold seawater and the temperature of the working fluid to ensure that the temperature changes of the seawater and the working fluid do not intersect [22]. Figure 3 shows the process chart of the study. Firstly, cycle process design was carried out to determine the composition and proportion of the working fluid. On this basis, 3-D design and CFD simulation analysis were used to obtain an efficient turbine meeting the operating conditions, and the off-working performance of the turbine was analyzed.

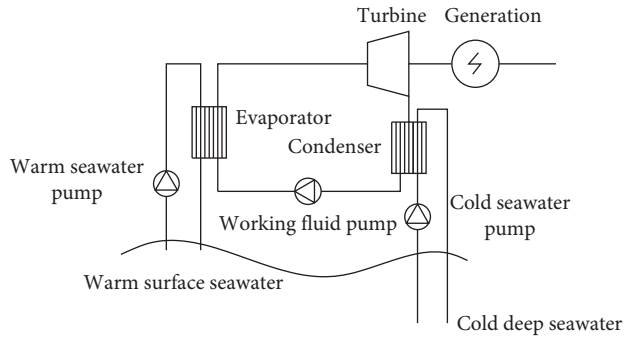

Figure 1: Diagram of OTEC ORC with zeotropic working fluid.

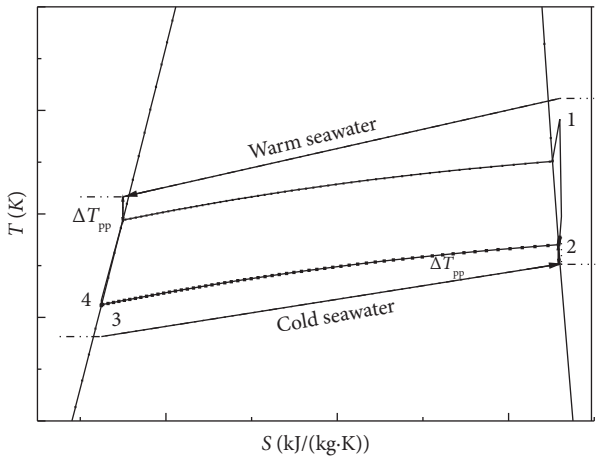

Figure 2: ORC with zeotropic working fluid in the T-S diagram.

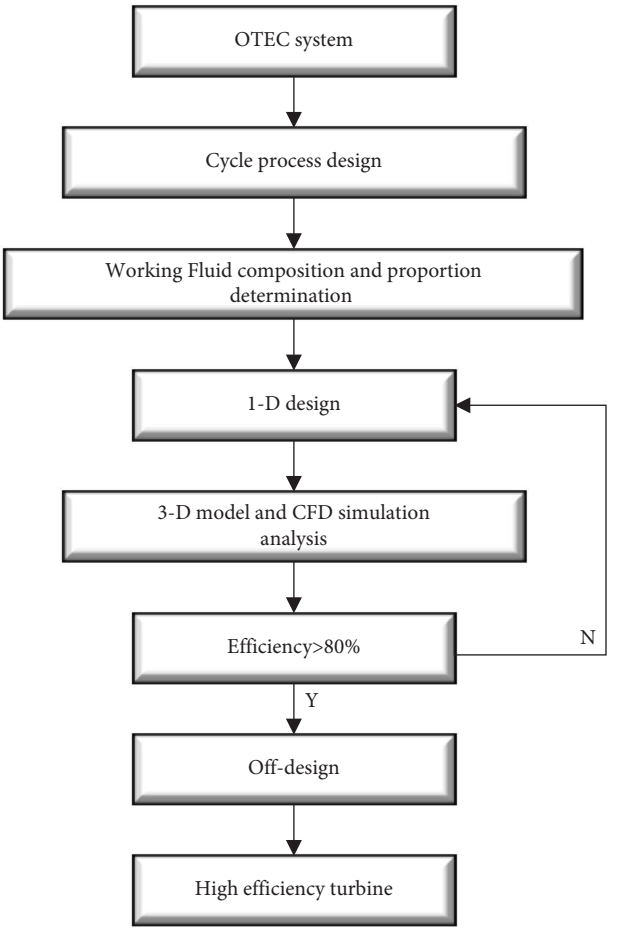

Figure 3: The process chart of the study.

2.2. Energy Conservation Model. The energy conversion model in this paper is based on the following assumptions:

(1) The working fluid is in steady-state flow, and each component is operated in a stable state;

(2) Heat exchange between each component and the environment is not considered;

(3) Leakage and clearance loss between components are not considered;

(4) The efficiency of the pump and turbine is constant;

the model is built according to the law of conservation of energy. During the evaporation process, the energy input to the system Q_{in} is the heat input of warm seawater, which is equal to the sum of the heat and loss required for the evaporation of the working fluid. During condensation, the energy output of the system Q_{out} is the sum of the heat and loss of the deep cold seawater heating.

$$\begin{aligned} Q_{in} &= M_{ws}C_{p,ws}\left(T_{ws,in} - T_{ws,out}\right) = M_{wf}\left(h_1 - h_4\right), \\ Q_{out} &= M_{cs}C_{p,cs}\left(T_{cs,out} - T_{cs,in}\right) = M_{wf}\left(h_2 - h_3\right), \end{aligned} \tag{1}$$

where M_{ws}, M_{cs}, and M_{wf} are warm seawater mass flow rate, cold seawater mass flow rate, and working fluid mass flow rate, respectively, kg/s. $C_{p,ws}$ and $C_{p,cs}$ are constant pressure specific heat capacity of warm seawater and constant pressure specific heat capacity of cold seawater in kJ/(kg·°C), respectively. $T_{ws,in}$ and $T_{cs,in}$ are warm seawater inlet temperature and cold seawater inlet temperature in °C, respectively; $T_{ws,out}$ and $T_{cs,out}$ are warm seawater outlet temperature and cold seawater outlet temperature, °C. h_1, h_2, h_3, are h_4 are the enthalpy values of the working fluid at the 1, 2, 3, and 4 state points, kJ·kg^{-1};

$$\begin{aligned} W_T &= M_{wf}\left(h_1 - h_2\right)W_{p,wf} = M_{wf}\left(h_4 - h_3\right), \\ W_{p,wf} &= M_{wf}\left(h_4 - h_3\right), \end{aligned} \tag{2}$$

where W_T and $W_{p,wf}$ are turbine output power and the power consumed by working fluid pump, kW.

Cycling thermal efficiency η_{cyc} and system thermal efficiency η_{sys} are important indicators for evaluating working fluids. A smaller temperature difference will definitely require more seawater, so the consumption of seawater pumps should not be ignored. In this paper, the cycle thermal efficiency and the system thermal efficiency will be considered comprehensively to finally determine the proportion of mixed working fluid components. The calculation formulas [29] are as follows:

$$\eta_{\mathrm{cyc}} = \frac{\left(W_{\mathrm{T}} - W_{\mathrm{p,wf}}\right)}{Q_{\mathrm{in}}},$$

$$\eta_{\mathrm{sys}} = \frac{\left(W_{\mathrm{T}} - W_{\mathrm{p}} - W_{\mathrm{p,sw}}\right)}{Q_{\mathrm{in}}},$$

$$\Delta H_{\mathrm{ws}} = \frac{6.82 \times L_{\mathrm{ws,sp}} \times \left(V_{\mathrm{ws}}/100\right)^{1.85}}{d_{\mathrm{ws,sp}}^{1.17} + 60 \times V_{\mathrm{ws}}^{2}/2g}, \tag{3}$$

$$\Delta H_{\mathrm{cs}} = \frac{6.82 \times L_{cs,sp} \times \left(V_{ws}/100\right)^{1.85}}{d_{\mathrm{cs,sp}}^{1.17} + 60 \times V_{\mathrm{cs}}^{2}/2g + L_{\mathrm{cs,sp}} - L_{\mathrm{cs,sp}} \times \left(\rho_{\mathrm{cs}} + \rho_{\mathrm{ws}}\right)/2\rho_{cs}},$$

$$d_{\mathrm{ws(cs),sp}} = \sqrt{\frac{4M_{\mathrm{ws(cs)}}}{\rho_{\mathrm{ws(cs)}}} \times \pi \times V_{\mathrm{ws(cs)}}},$$

where $W_{\mathrm{p,sw}}$ is seawater pump power, kW; $\Delta H_{\mathrm{w(c)s}}$ is total pressure head of warm (cold) seawater pump, m; $L_{\mathrm{w(c)s,sp}}$ is the length of warm (cold) seawater pipe, m; $d_{\mathrm{w(c)s,sp}}$ is the diameter of warm (cold) seawater pipe, m; $V_{\mathrm{w(c)s}}$ is the velocity of warm (cold) seawater in the pipe, m/s; $\rho_{\mathrm{w(c)s}}$ is warm(cold) seawater density, kg/m3; and g is the acceleration of gravity, m/s^2.

2.3. Determination of Working Fluid Components. As discussed above, binary zeotropic working fluids are more suitable for OTEC-ORC. One of the research objectives of this paper is to find a binary zeotropic working fluid suitable for OTEC systems to improve the system efficiency. First, the pure working fluid with better performance characteristics is screened out through literature investigation, including the physical parameters and thermodynamic properties, environmental protection indicators, safety performance, stability, and economy. Then, the ideal mixture model and the Peng Robinson (P-R) equation are employed in REFPROP 9.0 to calculate the thermodynamic properties of the mixture at different working fluid components. It is obvious to OTEC-ORC that different working fluid components will output different system efficiency and consume different pump power. The composition of the zeotropic working fluid is determined according to maximum efficiency. In the research of Li et al., the mixture with R32 as one of the components was proved to produce the largest specific net output power [28]. R32 was considered as an environmentally friendly refrigerant and adopted as a component of the working fluid mixture in the Yang and Yeh's research [22]. R152a was reported to have the highest thermal efficiency in OTEC-ORC and was safer than R717, operating at lower pressures without corrosion problems [30]. Based on the above principles for the selection of working fluid, R152a and R32 are initially selected as the components of the zeotropic working fluid due to their better thermodynamic properties, higher safety and stability, lower cost, and environmental friendliness.

Figure 4 shows the *T-S* diagrams of three working fluids, R152a, R32, and NH_3. They are all the wet working fluids, but R152a and R32 are much closer to the isentropic working fluid comparing to NH_3. In the enlarged view, it can be seen that R152a is the closest to the isentropic working fluid, which is beneficial to the operation of the turbine. Besides, compared to R32, R152a is more environmentally friendly, so it is better to choose R152a as the major component for the working fluid mixture.

2.4. Determination of the Composition of the Working Fluid. Aspen Plus V9 is used to simulate the OTEC ORC, based on which all thermodynamic parameters at each key node of the cycle can be obtained to calculate cycle efficiency and system efficiency. First, the thermodynamic cycle was established according to the initial conditions of each node shown in Table 1. Next, the physical parameters of the working fluid are determined though the simulation based on the PR state equation. Then, important data such as the mass flow of warm and cold seawater, turbine inlet and outlet pressures, etc., are obtained. The temperature glide in the evaporation and condensation processes of the working fluid are then calculated based on the data from Aspen and REFPROP 9.0, and the cycle efficiency and system efficiency can be calculated according to equations in Section 2.2. By comprehensively consider the temperature glides and the thermal efficiencies, the optimal composition of the nonazeotropic mixture of R152a/R32 can be determined.

Figure 5 displays the effect of the ratio of R152a to R32 on the temperature glide and the superheat degree at the turbine inlet. The temperature glide during evaporation and condensation is similar. There is no temperature glide in pure working fluid, when the mass fraction of R152a is equal to 0 or 1. When the mass fraction of R152a is about 0.55, the temperature glide of evaporation and condensation is close to the maximum value of 8°C. In addition, the superheat degree of NH_3 is about 9°C, while that of R152a/R12 mixture has a maximum superheat of about 8°C at 0.1/0.9, indicating that the zeotropic working fluid composed of R152a and R32 has better heat utilization potential than NH_3. The superheat degree of R152a/R32 is relatively small, in the range of 0.5 to 1, so the mass fraction of R152a should be within this range.

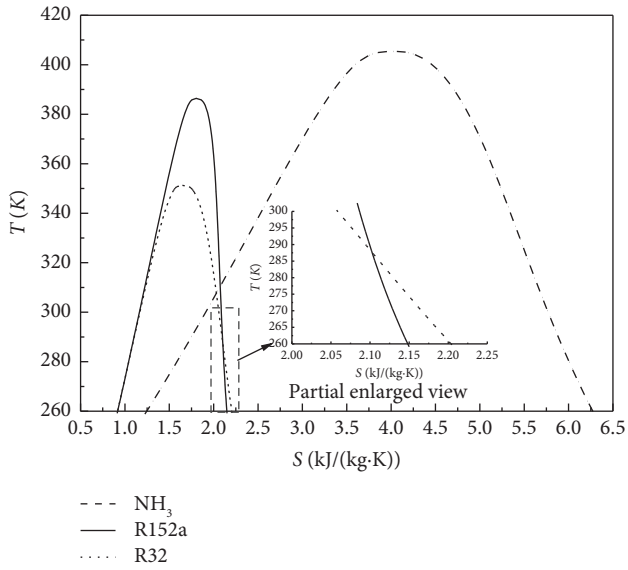

Figure 4: *T*-*S* diagram of three working fluids.

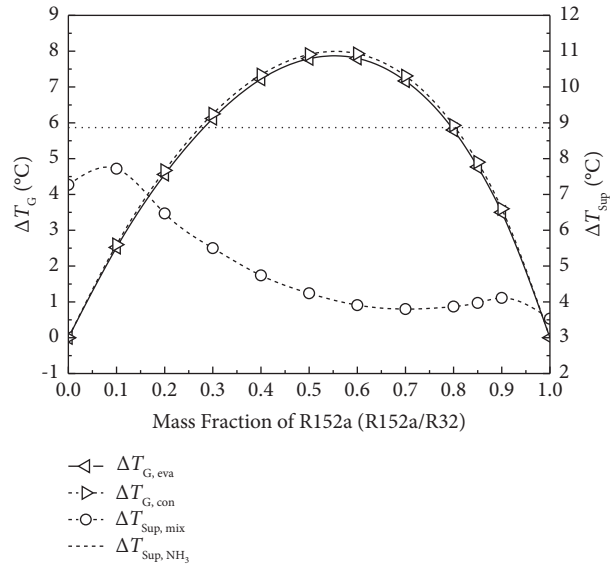

Figure 5: Temperature glide and superheated degree.

Table 1: The main parameters and 1-D design results.

Parameters	Units	Values	Parameters	Units	Values
$T_{ws,in}$	℃	28	$T_{cs,in}$	℃	5
$T_{turb,in}$	℃	26	$T_{con,out}$	℃	7
$p_{turb,in}$	MPa	0.623	$p_{turb,out}$	MPa	0.453
M_{wf}	kg/s	9.13	W_T	kW	100
χ_a	—	0.707	η_T	—	0.9
α_1	°	14°	$\overline{D}$	—	0.42
β_2	°	30°	Ψ	—	0.85
Ω	—	0.5	φ	—	0.96
c_{2ss}	m/s	148.01	$D_{r,hub}$	m	0.0579
c_1	m/s	100.47	$D_{r,out,m}$	m	0.1527
u_1	m/s	104.64	$l_{r,out}$	m	0.0750
w_1	m/s	25.34	$\delta_{s,r}$	m	0.0013
c_2	m/s	25.37	L_{rx}	m	0.120
u_2	m/s	43.95	$D_{n,in}$	m	0.452
w_2	m/s	50.75	$D_{n,out}$	m	0.364
N_r	—	15	$r_{v,in}$	m	0.05174
N_n	—	24	$r_{t,max}$	m	0.3305
Re_{t1}	—	6.6732×10^7	L_d	m	0.075
μ_1	Pa·s	1.0514×10^{-5}	L_{tx}	m	0.225
$D_{r,in}$	M	0.3635	η_u	—	0.8148
N	rpm	5498.55	$\eta_{t,isen}$	—	0.7601
$A_{r,out}$	m^3	0.0313	ζ_l	—	0.03842
$D_{r,shroud}$	m	0.208	ζ_f	—	0.01625

Figure 6 demonstrates the effect of the mass fraction of R152a on the thermal efficiency of OTEC-ORC in the saturated and superheated state. The R152a/R32 with the composition of 0.1 : 0.9 in saturation can be chosen as the working fluid of OTEC-ORC to obtain the maximum thermal efficiency of about 5.26% which is higher than the NH_3 ORC by 11.4%. In a previous study [24], we found that R1224yd(Z)/R1243zf achieved a cyclic thermal efficiency of 4.25%, but now the maximum cyclic thermal efficiency of R152a/R32 is 23.8% higher than that of R1224yd(Z)/R1243zf at saturation. Although the thermal efficiency of R152a/R32 ORC and the NH_3 ORC is higher in a saturated state than in a superheated state, the problem of droplets in a saturated state is unavoidable. Therefore, superheated state should be adopted. The thermal efficiency with R152a/R32 is higher than that of NH_3 at any mass fraction when the steam at the turbine inlet is superheated. The R152a/R32 mixture with a composition of 0.9/0.1 can be selected to obtain a maximum thermal efficiency of about 3.1%, nearly twice of that of NH_3 ORC.

The energy consumption of the seawater pump is one of the factors that needs to be considered in OTEC-ORC. In order to meet the need for electricity generation, the consumption of the seawater pump should be less than the output power of the system. Figure 7 reveals the power consumption of the seawater pump at seawater velocity of 1 m/s, 1.5 m/s, and 2 m/s, respectively. It can be seen from the figure that, as the seawater flow rate increases, the work consumed by the sea water pump also increases. Regardless of the seawater flow rate, when the mass fraction of R152a is in the range of 0.1~0.9, the energy consumption of the seawater pump changes gently, which is closely related to the temperature glide of zeotropic mixtures, due to which the heat transfer between the working fluid and seawater matches better. Oppositely, there is no temperature glide during evaporation and condensation of pure NH_3, R152a, and R32. Thus, more seawater is needed as the heat sources and the power consumption of a seawater pump is more significant.

Figure 8 presents the system efficiency of R152a/R32 ORC and NH_3 ORC based OTEC plant at seawater velocity of 1 m/s, 1.5 m/s, and 2 m/s, respectively. In the previous study [24], the system efficiency of R1224yd(Z)/R1243zf reached 3.23%, while the system efficiency of R152a/R32 was only 2.44%, because we ensured that R152a/R32 was overheated throughout the cycle. At the same velocity, the system efficiency of R152a/R32 ORC is always higher than

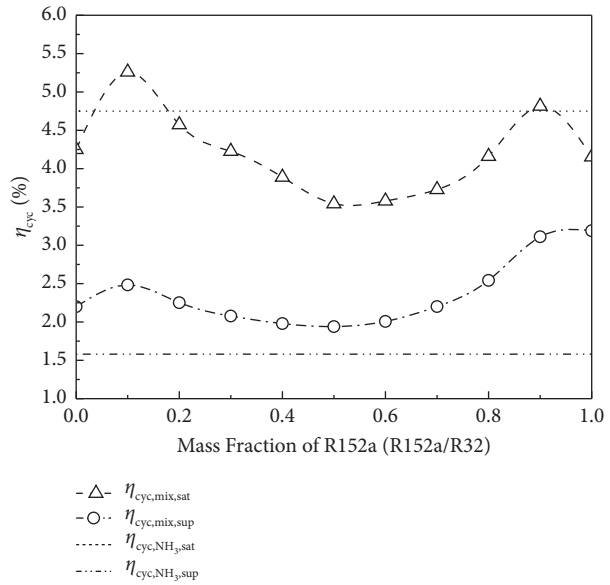

Figure 6: Thermal efficiency of OTEC-ORC with R152a/R32 and NH_3 as working fluids in a superheated and saturated state.

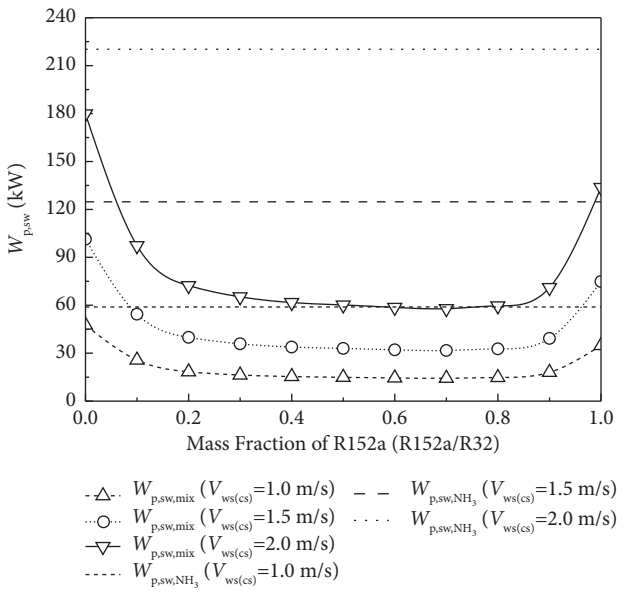

Figure 7: Power consumption of seawater pumps under different seawater velocities in the pipeline.

that of NH_3 ORC. The system efficiency is the highest at velocity of 1.0 m/s, and the zeotropic working fluid achieves a maximum system efficiency of 2.44% when the mass fraction R152a is about 0.9, improved by 354% compared to NH_3 ORC. With the increase of seawater velocity, the efficiency of the system decreases. When the seawater flow rate is greater than or equal to 2 m/s, the system efficiency is approaching to 0 or even negative, which means that the OTEC system consumes similar or more energy than the supply. Such an OTEC plant is not allowed in the application. Although reducing the seawater flow rate is an effective way to improve the efficiency of the system, the accompanying pipe enlargement should also be considered. It will cost more and the installation and maintenance will become more difficult. In this paper, the seawater flow rate in the pipe is set to be 1.5 m/s, by comprehensively considering the efficient power generation, system efficiency, and application difficulties. At this velocity, the system efficiency achieves the maximum when the mass fraction of R152a is 0.85, achieves, so the proportion of R152a/R32 is finally determined to be 85 : 15.

3. 1-D Design of the OTEC-ORC Turbine

The design parameters such as turbine inlet temperature and pressure are obtained by cycle simulation using Aspen plus V9 software and the 1-D design calculation of the turbine is carried out according to the literature [31–37]. The results are shown in Table 1.

4. CFD Simulation of OTEC-ORC Turbine

Based on 1-D design results, CFturbo, the professional rotating machinery modeling software, is employed to generate the geometrical model of the turbine in the OTEC-ORC with R152a/R32 as working fluid. Figure 9 presents the 3-D model of the turbine, which is divided into four parts: volute, nozzle, impeller, and diffuser. The working fluid is guided through the volute, accelerated in the nozzle, then goes into the impeller to generate rotation, and finally flows out of the diffuser. The volute, the nozzle, and the diffuser are static, and the impeller is rotated. The nozzle and impeller are axisymmetric, so the periodic boundaries are adopted to simplify the model.

4.1. Control Equations and Boundary Conditions. The R152a/R32 binary zeotropic mixture with a mass fraction ratio of 0.85 : 0.15 is the working fluid of the turbine. The ideal mixture model is adopted to calculate the thermodynamic properties of the mixture. The Peng Robinson (4) is adopted to calculate the state of the working fluid.

$$p = \frac{\mathrm{RT}}{V-b} - \frac{\alpha(T)}{V(V+b)+b(V-b)}, \tag{4}$$

where b is the constant related to the critical parameter.

In addition, CFD simulation is governed by continuity (5), momentum (6), and energy (7), using the k-ε equation (8), (9) to analyze the turbulence. The boundary conditions used in this study are total pressure inlet and static pressure outlet, since pressure control is easily realized in practice. Wall slip is ignored, and the adiabatic boundary conditions are applied to the hub, shroud, and walls. Moreover, the necessary periodic boundaries are set to the nozzle and impeller to reduce the mesh number.

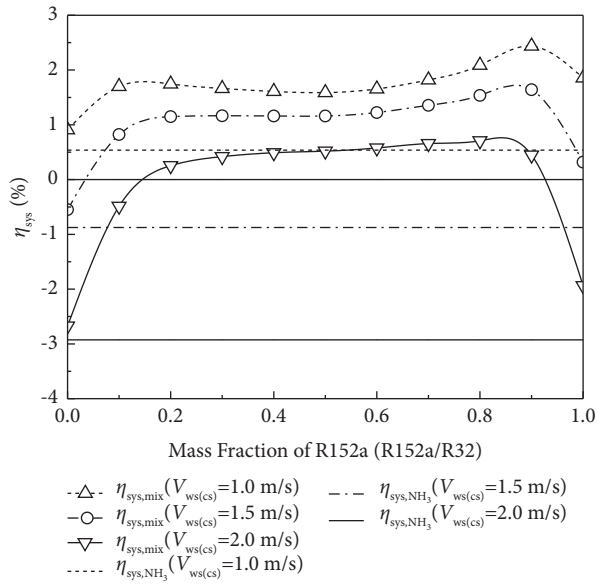

Figure 8: System efficiency of R152a/R32 and NH_3 under different seawater velocities in the pipeline.

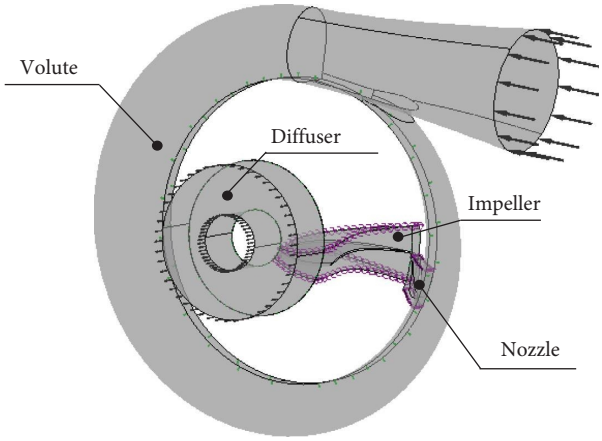

Figure 9: Runner model of the radial inflow turbine.

$$\frac{\partial \rho}{\partial t} + \nabla \cdot (\rho U) = 0, \tag{5}$$

$$\rho \frac{d\mathbf{v}}{dt} = -\nabla p + \rho \mathbf{F} + \mu \Delta \mathbf{v}, \tag{6}$$

$$\frac{\partial \rho}{\partial t} + \nabla \cdot (\rho U \otimes U) - \nabla \cdot \left(\mu_{\text{eff}} \nabla U\right) = \nabla \cdot p' + \nabla \cdot \left(\mu_{\text{eff}} \nabla U\right)^T + B, \tag{7}$$

$$\frac{\partial \rho k}{\partial t} + \nabla \cdot (\rho U k) = \nabla \cdot \left[\left(\mu + \frac{\mu_t}{\sigma_k}\right) \nabla k\right] + P_k - \rho \varepsilon, \tag{8}$$

$$\frac{\partial (\rho \varepsilon)}{\partial t} + \nabla \cdot (\rho U \varepsilon) = \nabla \cdot \left[\left(\mu + \frac{\mu_t}{\sigma_\varepsilon}\right) \nabla \varepsilon\right] + \frac{\varepsilon}{k} \left(C_{\varepsilon 1} P_k - C_{\varepsilon 2} \rho \varepsilon\right), \tag{9}$$

(a) (b) (c) (d)

Figure 10: Mesh of the turbine component. (a) Volute, (b) Nozzle (c) Impeller (d) Diffuser.

where μ_{eff} and B are the effective viscosity and the total body force respectively; σ_k, σ_ε, $C_{\varepsilon 1}$, and $C_{\varepsilon 2}$ are constants, and P_k are the products of viscous force and buoyancy force.

4.2. Meshing and Grid Independence Analysis. Figure 10 shows the mesh of the turbine model. The Mesh toolbox is employed to generate the mesh of the volute and diffuser for their simple structures, and TurboGrid is applied for constructing high-quality grids for impeller and nozzle, which are key components of the turbine and have a significant influence on the isentropic efficiency of the turbine. Grid independence analysis is required to ensure the accuracy and efficiency of simulation, and the final results are depicted in Figure 11. The output power and efficiency of turbine fluctuates with the increase of the total number of grid. The output power and efficiency are stabilized at a grid size of about 1.15 million. Finally, the total number of meshes for the turbine is 1149797, including 198795 for volute, 494832 for nozzle, 337053 for impeller, and 119117 for diffuser.

4.3. Influence Analyses of Operating Parameters

4.3.1. Influence of Rotational Speed of the Impeller. Figure 12 depicts the effect of rotational speed of the impeller on the turbine's performance. The output power and isentropic efficiency both vary in a parabolic shape with the rotational speed within the range from 4000 rpm to 7000 rpm. At the design point, the output power reaches its maximum, and the isentropic efficiency is 87.47%. The isentropic efficiency is 87.99% reaching the maximum at 6000 rpm, but the mass flow rate and output power deviated from the design point by 4.16% and 13.48%, which cannot meet the design requirement. Figure 13 shows distribution of Mach number at the half blade height with different rotational speed of impeller. As the speed increases, the maximum of the drops but the vortex in the impeller weakens, their combined action resulting in the parabolic curve of the power and efficiency variation. In addition, with the decrease of the Mach number, the velocity of the vapor decreases too, resulting in the reduction of the mass flow rate.

4.3.2. Influence of Mass Flow Rate. Figure 14 shows the effect of the mass flow rate of the working fluid on the output power and isentropic efficiency of the turbine. The mass flow rate varies from 8 kg/s to 10.5 kg/s, and the designed value is 9.13 kg/s. The flow outlet instead of static pressure outlet is used to ensure the accuracy of the mass flow rate. The output power increases with the mass flow, the turbine outlet pressure decreases continuously, and the isentropic efficiency shows a trend of increasing first and then decreasing. When the mass flow rate is 9 kg/s, the isentropic efficiency reaches the maximum value of 88.27%, and the deviation from the design point is only 1.92%. Figure 15 shows the influence of the mass flow rate on Mach number at the half blade height. As the mass flow rate increases, Mach number increase obviously due to the vapor velocity rise which also results in an increase of the power output. Meanwhile, the higher the Mach number, the more flow loss and friction loss it causes, so the efficiency of the turbine decreases accordingly.

4.3.3. Influence of Turbine Inlet Temperature. The turbine inlet temperature will fluctuate with the surface seawater temperature. When the surface seawater temperature changes, the turbine inlet temperature should be adjusted to maintain the necessary pinch point. Meanwhile, the turbine inlet pressure should be updated to ensure no droplets condensate in the turbine.

Figure 16 shows the effect of turbine inlet temperature on output power and isentropic efficiency, as well as the turbine inlet pressure. With the increase of turbine inlet temperature, the variation of isentropic efficiency is not obvious, while a significant increase occurs in output power due to the increasing pressure at the turbine inlet. The turbine can be operated efficiently near the design point, which shows that our design is highly resistant to fluctuations of turbine inlet temperature. Furthermore, if feasible, coupling with other heat sources with OTEC to increase the turbine inlet temperature will be helpful to improve output power. Figure 17 shows the effect of turbine inlet temperature on Mach number at half the blade height. The influence is not significant, so the efficiency of the turbine is hardly affected by the turbine inlet temperature, indicating the turbine has good off-design performance as well.

4.4. On and Off-Design Performance Analysis. The simulated design points of the turbine are marked in

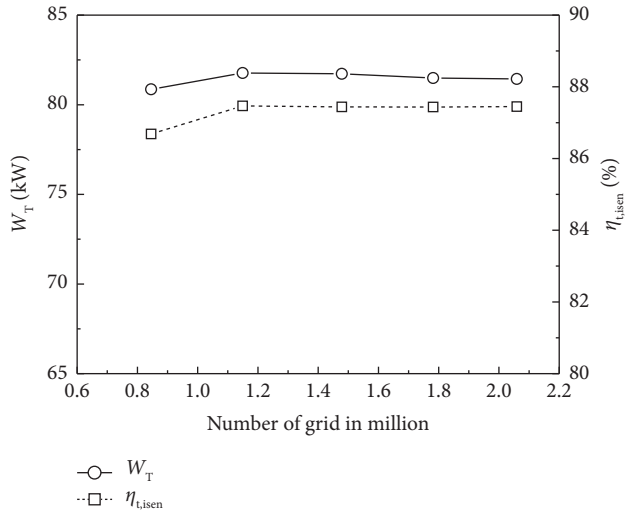

Figure 11: The result of grid independence analysis.

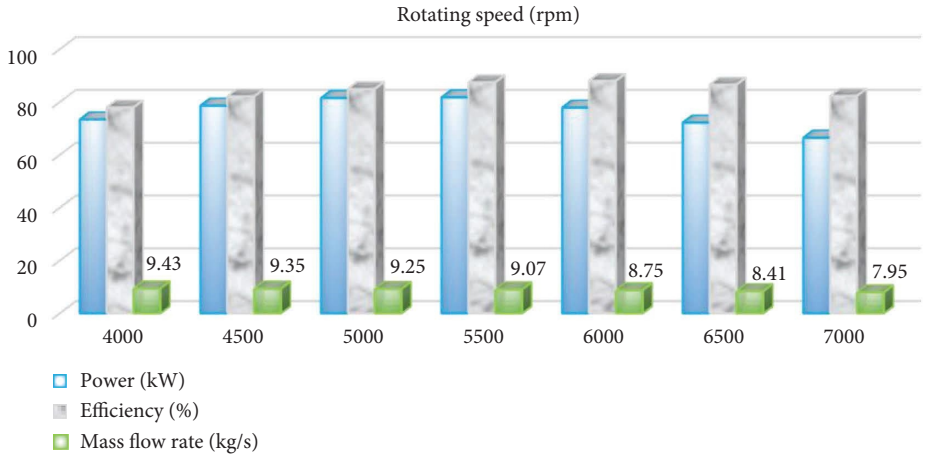

Figure 12: The influence of rotational speed of impeller.

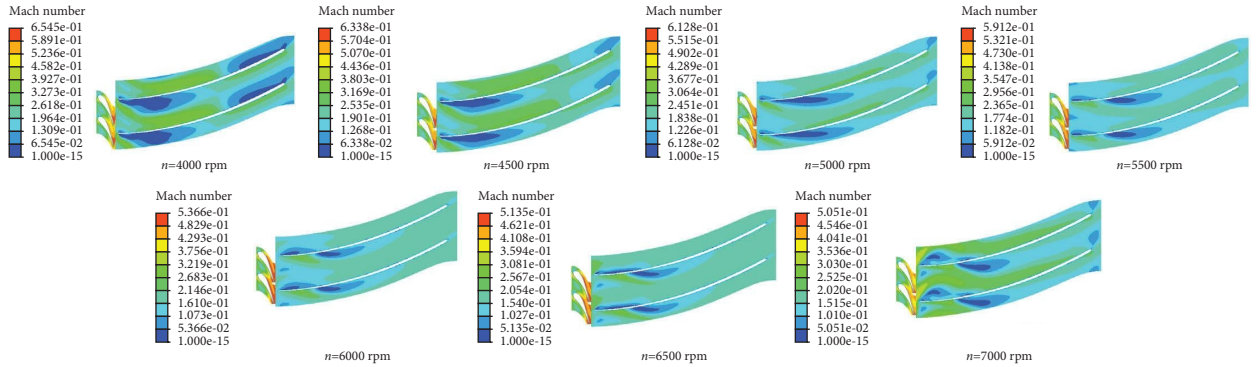

Figure 13: Distribution of Mach number at the half blade height with rotational speed of impeller.

Figures 11–13. At the design point, the turbine inlet pressure, turbine inlet temperature, the turbine outlet pressure, the mass flow rate and the rotational speed of the impeller are 0.623 MPa, 26°C, 9.13 kg/s and 5500 rpm, respectively. The output power and the isentropic efficiency can achieve 83.84 kW and 87.53%, deviated from

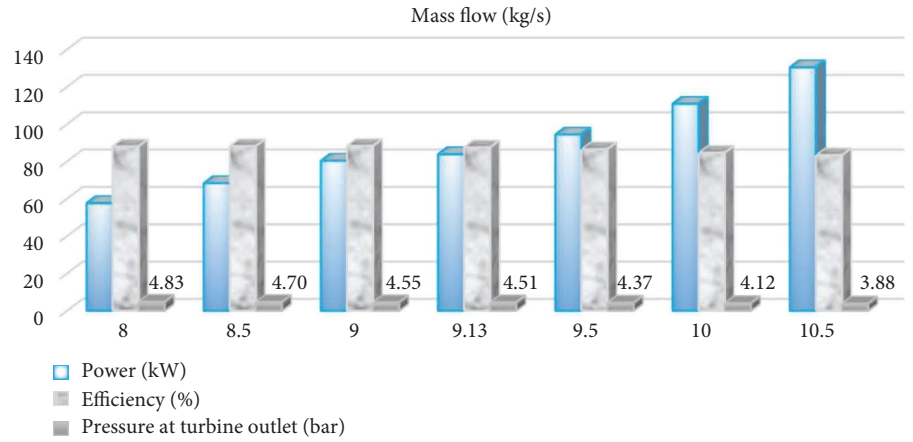

Figure 14: The influence of mass flow rate.

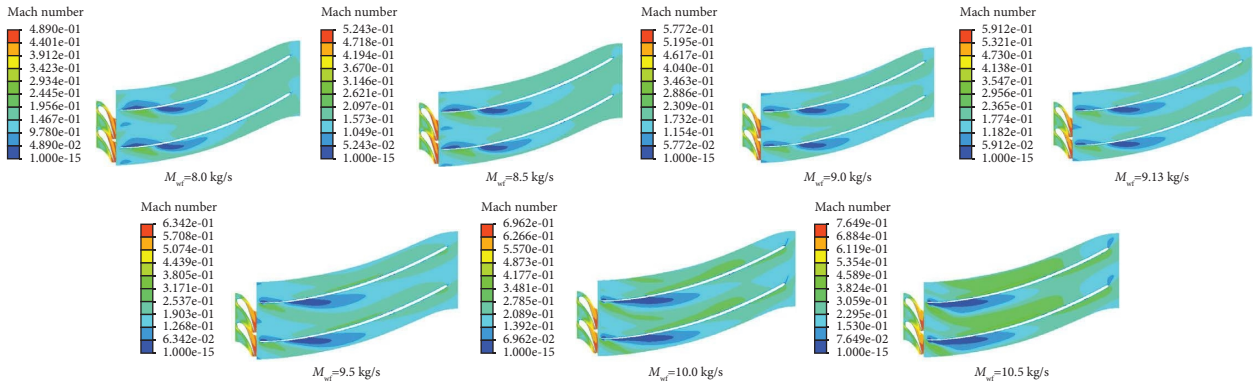

Figure 15: Distribution of Mach number at the half blade height with mass flow rate.

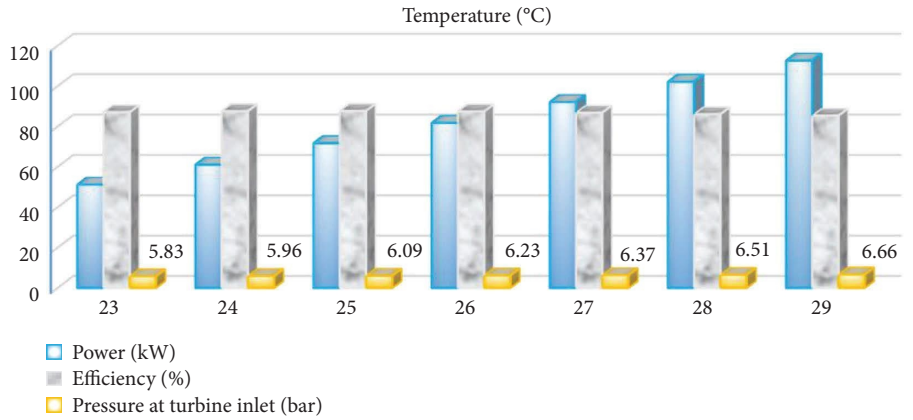

Figure 16: The influence of turbine inlet temperature.

the 1-D results by only 6.84% and 2.74%, indicating a good agreement with the 1-D calculation.

No matter what kind of equipment, fluctuations in operation are unavoidable. Dynamic balance is one of the indicators to judge whether a device is applicable. Regardless of the variation in investigated operating parameters, the turbine achieves high efficiency close to the design point, indicating good off-design performance of the turbine.

When the deviation of the turbine inlet temperature is within 11.5%, the isentropic efficiency of the turbine can be maintained near the design point, and the maximum deviation is 2.38%. When the deviation of the rotational speed

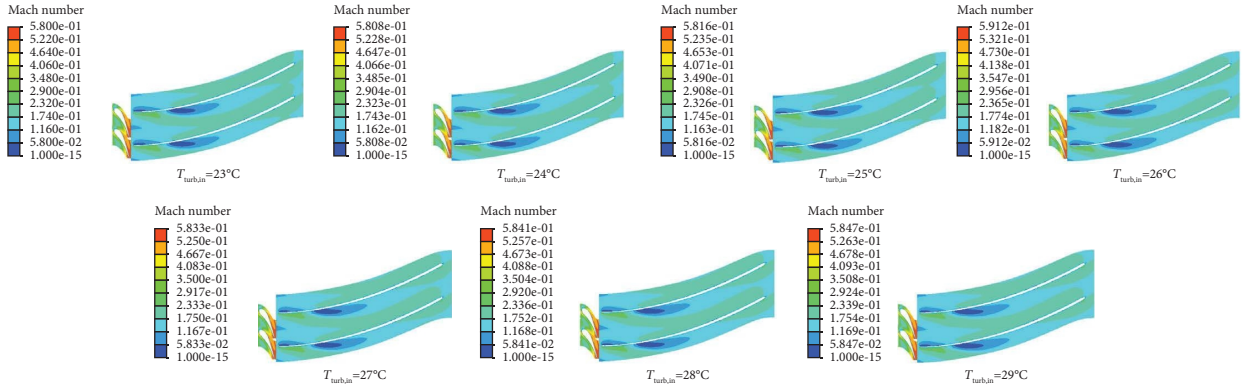

Figure 17: Distribution of Mach number at the half-blade height with turbine inlet temperature.

of the impeller is within 16.7%, the maximum deviation of isentropic efficiency is 10.9%. The maximum efficiency deviation is 4.77% when the mass flow rate varies from 8 kg/s to 10.5 kg/s.

Therefore, it can be said that the turbine designed in this paper has good off-design performance.

5. Conclusions

To improve the energy conversion rate of OTEC-ORC, the suitable zeotropic working fluid and the turbine are investigated by thermodynamic analysis, theoretical design, and CFD simulation. The following conclusions can be obtained.

(1) R152a and R32 mixture has good potential to replace the common working fluid of OTEC-ORC; whether saturated or superheated, R152a/R32 are more efficient than ammonia. The optimal composition of R152a/R32 is 85/15, at which maximum of the system efficiency can be achieved.

(2) The turbine with R152a/R32 (85/15) as the working fluid is designed, theoretically calculated and verified by CFD simulation. The 1-D theoretical calculation results match well with the CFD simulation results, and the turbine performs well at the design point. The influences of the inlet temperature of the turbine, the speed of the impeller, and the mass flow rate of the working fluid are investigated, indicating good off-design performance.

(3) In this study, enough superheated degree was present at the turbine inlet to ensure 100% of any droplet did not form in the turbine. In the future, the nonisentropic operation of the turbine and the supercooling degree of the nucleation both should be considered in specific to obtain the inlet pressure of turbine more accurately so that the output can be improved further under the limited condition of the OTEC. In addition, the matching of the power generation scale and zeotropic working fluid body is also a problem worth considering.

Nomenclature

A_R: Area ratio
b_4: Rotor outlet blade width (mm)
c: Absolute speed (m/s)
u: Tangential velocity (m/s)
w: Relative velocity (m/s)
W: Power (kW)
m: Mass flow rate (kg/s)
n: Rotational speed (rpm)
Re: Reynolds number
T: Temperature
Z: Number
L: Length (mm)
D: Diameter

Greek letter

α: Absolute airflow angle
β: Relative airflow angle
χ: Characteristic ratio
φ: Nozzle velocity coefficient
ψ: Rotor velocity coefficient
$\overline{D}$: Ration of wheel diameter
Ω: Reaction degree
ξ: Loss
η: Efficiency
Δ: Different

Subscripts

turb: Turbine
con: Condenser
eva: Evaporator
in: Inlet
out: Outlet
ws: Warm seawater
cs: Cool seawater
r: Rotor
n: Nozzle
1,2,3,4: State point in cycle
sys: System
p: Pump
T: Theory
sat: Saturated state
sup: Superheated state

x: Axial
wf: Working fluid
v: Volute
isen: Isentropic

Acronyms

ORC: Organic rankine cycle
OTEC: Ocean thermal energy conversion
CFD: Computational fluid dynamics
ORC: Oganic rankine cycle
1-D: One-dimensional
3-D: Three-dimensional
P-R: Peng Robinson

Data Availability

The [DATA TYPE] data used to support the findings of this study are included within the article and are also available from the corresponding author upon request.

Conflicts of Interest

The authors declare that they have no conflicts of interest.

Acknowledgments

This work was financially supported by the Hainan Province Science and Technology Special Fund (ZDYF2021GXJS021), the Hainan Provincial Natural Science Foundation of China (520RC533 and 422CXTD509), and the National Natural Science Foundations of China (51769006).

References

[1] D. S. Li, Q. Liu, and F. Dong, "Technical progress and foresight research on development and utilization of marine thermal energy," *Industrial heating*, vol. 50, no. 11, pp. 1–3+16, 2021.

[2] H. W. Zhang, X. H. Ma, and Y. N. Yang, "An external ocean thermal energy power generation modular device for powering smart float," *Energies*, vol. 15, no. 10, p. 3747, 2022.

[3] Y. H. Wu, H. H. Lv, and Y. U. Ting, "Research on power system scheme of 10MW Marine thermogenic power station," *Ocean Engineering Equipment and Technology*, vol. 9, no. 1, pp. 46–51, 2022.

[4] A. Hasan and I. Dincer, "A new integrated ocean thermal energy conversion-based trigeneration system for sustainable communities," *Journal of Energy Resources Technology*, vol. 142, no. 6, 2020.

[5] T. Du, Z. Jing, L. Wu et al., "Growth of ocean thermal energy conversion resources under greenhouse warming regulated by oceanic eddies," *Nature Communications*, vol. 13, no. 1, p. 7249, 2022.

[6] A. Hasan and I. Dincer, "An ocean thermal energy conversion based system for district cooling, ammonia and power production," *International Journal of Hydrogen Energy*, vol. 45, no. 32, pp. 15878–15887, 2020.

[7] H. Y. Wu, J. P. Peng, and Y. Z. Ge, "Performance analysis of an efficient marine thermoelectric power generation cycle," *Progress in Marine Science*, vol. 38, no. 3, pp. 513–521, 2020.

[8] C. Bernardoni, M. Binotti, and A. Giostri, "Techno-economic analysis of closed OTEC cycles for power generation," *Renewable Energy*, vol. 132, pp. 1018–1033, 2019.

[9] I. S. Arief and D. R. Aldara, "Preliminary Design of Ocean Thermal Energy Conversion (OTEC) Axial Turbine for Laboratory Scale," in *Proceedings of the 2018 Asian Conference on Energy, Power and Transportation Electrification (ACEPT)*, pp. 1–8, IEEE, Singapore, October 2018.

[10] S. Li, X. Zhai, Y. Liu, W. Liu, L. Wang, and J. Zhang, "Effects of working conditions on the performance of an ammonia ejector used in an ocean thermal energy conversion system," *Canadian Journal of Chemical Engineering*, vol. 99, no. 12, pp. 2723–2736, 2021.

[11] Q. Y. He, Q. Liu, and D. S. Li, "Study on the coupling of cold storage refrigeration and marine thermoelectric power generation system," *Journal of Marine Technology*, vol. 41, no. 4, pp. 106–111, 2022.

[12] D. Vera, A. Baccioli, F. Jurado, and U. Desideri, "Modeling and optimization of an ocean thermal energy conversion system for remote islands electrification," *Renewable Energy*, vol. 162, pp. 1399–1414, 2020.

[13] C. Zhang, Z. Wu, J. Wang, C. Ding, T. Gao, and Y. Chen, "Thermodynamic performance of a radial-inflow turbine for ocean thermal energy conversion using ammonia," *Renewable Energy*, vol. 202, pp. 907–920, 2023.

[14] B. Li, L. Zhang, M. H. Xu, and D. S. Li, "Development of OTEC Rankine cycle thermal calculation software with R134a as working fluid," *Thermal Science and Technology*, vol. 21, no. 4, pp. 403–414, 2022.

[15] J. I. Yoon, C. H. Son, S. M. Baek, H. J. Kim, and H. S. Lee, "Efficiency comparison of subcritical OTEC power cycle using various working fluids," *Heat and Mass Transfer*, vol. 50, no. 7, pp. 985–996, 2014.

[16] D. S. Li and L. Zhang, "Numerical analysis on evaporating pressure and working fluids of ocean thermal energy conversion," *Renewable Energy Resources*, vol. 35, no. 7, pp. 1101–1106, 2017.

[17] T. Morisaki and Y. Ikegami, "Performance evaluation of heat exchangers in OTEC using ammonia/water mixture as working fluid," *Open Journal of Fluid Dynamics*, vol. 3, no. 04, pp. 302–310, 2013.

[18] A. I. Kalina, "Combined-cycle system with novel bottoming cycle," *Journal of Engineering for Gas Turbines & Power*, vol. 106, no. 4, pp. 737–742, 1984.

[19] H. Uehara, "Performance analysis of OTEC system using a cycle with absorption and extraction processes," *Transaction of JSME, Serie Bibliographique*, vol. 64, no. 624, pp. 384–389, 1998.

[20] W. M. Liu, F. Y. Chen, Y. Q. Wang, W. J. Jiang, and J. G. Zhang, "Progress of closed-cycle OTEC and study of a new cycle of OTEC," *Advanced Materials Research*, vol. 354-355, no. 1, pp. 275–278, 2011.

[21] W. Liu, X. Xu, F. Chen et al., "A review of research on the closed thermodynamic cycles of ocean thermal energy conversion," *Renewable and Sustainable Energy Reviews*, vol. 119, Article ID 109581, 2020.

[22] M. H. Yang and R. H. Yeh, "Investigation of the potential of R717 blends as working fluids in the organic Rankine cycle (ORC) for ocean thermal energy conversion (OTEC)," *Energy*, vol. 245, Article ID 123317, 2022.

[23] M. H. Yang and R. H. Yeh, "The investigation of optimum multi-component blends in organic Rankine cycle for ocean thermal energy conversion," *Applied Thermal Engineering*, vol. 217, Article ID 119279, 2022.

[24] Q. Ma, Z. Gao, J. Huang et al., "Thermodynamic analysis and turbine design of a 100 kW OTEC-ORC with binary non-

azeotropic working fluid," *Energy*, vol. 263, Article ID 126097, 2023.

[25] J. I. Yoon, C. H. Son, S. H. Seol et al., "Performance analysis of OTEC power cycle with a liquid vapor ejector using R32/R152a," *Heat and Mass Transfer*, vol. 51, no. 11, pp. 1597–1605, 2015.

[26] H. Chen, D. Y. Goswami, and E. K. Stefanakos, "A review of thermodynamic cycles and working fluids for the conversion of low-grade heat," *Renewable and Sustainable Energy Reviews*, vol. 14, no. 9, pp. 3059–3067, 2010.

[27] A. Schuster, S. Karellas, E. Kakaras, and H. Spliethoff, "Energetic and economic investigation of organic rankine cycle applications," *Applied Thermal Engineering*, vol. 29, no. 8-9, pp. 1809–1817, 2009.

[28] C. Li, L. Pan, and Y. Wang, "Thermodynamic optimization of Rankine cycle using CO_2-based binary zeotropic mixture for ocean thermal energy conversion," *Applied Thermal Engineering*, vol. 178, Article ID 115617, 2020.

[29] S. Zhou, X. Liu, K. Zhang, Q. Yue, Y. Bian, and S. Shen, "Evaluation of a novel ammonia-water based combined cooling, desalination and power system based on thermodynamic and exergoeconomic analyses," *Energy Conversion and Management*, vol. 239, Article ID 114176, 2021.

[30] F. Chen, L. Liu, J. Peng, Y. Ge, H. Wu, and W. Liu, "Theoretical and experimental research on the thermal performance of ocean thermal energy conversion system using the rankine cycle mode," *Energy*, vol. 183, pp. 497–503, 2019.

[31] G. H. Ji, *Turbine Expander*, China Machine Press, Beijing, China, 1982.

[32] Z. Wu, H. Feng, L. Chen, Z. Xie, C. Cai, and S. Xia, "Optimal design of dual-pressure turbine in OTEC system based on constructal theory," *Energy Conversion and Management*, vol. 201, Article ID 112179, 2019.

[33] L. S. Pan and H. X. Wang, "Improved analysis of organic Rankine cycle based on radial flow turbine," *Applied Thermal Engineering*, vol. 61, no. 2, pp. 606–615, 2013.

[34] C. A. M. Ventura, P. A. Jacobs, A. S. Rowlands, P. Petrie-Repar, and E. Sauret, "Preliminary design and performance estimation of radial inflow turbines: an automated approach," *Journal of Fluids Engineering*, vol. 134, no. 3, pp. 31102–31111, 2012.

[35] H. Moustapha, M. F. Zelesky, N. C. Baines, and D. Japikse, *Axial and Radial Turbines White River Junction*, Concepts NREC, Bengaluru, India, 2003.

[36] K. Rahbar, S. Mahmoud, R. K. Al-Dadah, and N. Moazami, "Parametric analysis and optimization of a small-scale radial turbine for Organic Rankine Cycle," *Energy*, vol. 83, pp. 696–711, 2015.

[37] J. Xia, J. Wang, H. Wang, and Y. Dai, "Three-dimensional performance analysis of a radial-inflow turbine for an organic Rankine cycle driven by low grade heat source," *Energy Conversion and Management*, vol. 169, pp. 22–33, 2018.